

Structural Behavior of the Four-Layer Aurivillius-Phase Ferroelectrics $\text{SrBi}_4\text{Ti}_4\text{O}_{15}$ and $\text{Bi}_5\text{Ti}_3\text{FeO}_{15}$

Charles H. Hervoches,* Alan Snedden,* Richard Riggs,* Susan H. Kilcoyne,†
Pascal Manuel,† and Philip Lightfoot*¹

*School of Chemistry, University of St. Andrews, St. Andrews, Fife, KY16 9ST, United Kingdom; and †School of Physics, University of Leeds, Leeds, LS2 9JT, United Kingdom

Received July 25, 2001; in revised form November 15, 2001; accepted December 3, 2001

Rietveld refinement of powder neutron diffraction data has been used to study the crystal structures of the four-layer Aurivillius-phase ferroelectrics $\text{Bi}_5\text{Ti}_3\text{FeO}_{15}$ (at 25°C) and $\text{SrBi}_4\text{Ti}_4\text{O}_{15}$ (at a series of temperatures up to 800°C). At 25°C both materials adopt the polar orthorhombic space group $A2_1am$, in common with two-layer analogues such as $\text{SrBi}_2\text{Ta}_2\text{O}_9$. At temperatures well above the ferroelectric Curie temperature (i.e., at temperatures of 650°C and above, with $T_c \sim 550^\circ\text{C}$) $\text{SrBi}_4\text{Ti}_4\text{O}_{15}$ transforms to the centrosymmetric tetragonal space group $I4/mmm$. However, there is good evidence from the raw diffraction data of a very subtle intermediate paraelectric orthorhombic phase, of $Amam$ symmetry, in the region $550 > 650^\circ\text{C}$. The distortion in the ferroelectric phase can be traced to displacements of the cations in the A site of the perovskite block, with cooperative tilting of the BO_6 octahedra. The nature of the octahedral tilt system, cation disorder at the perovskite A and B sites, and the phase transition sequence in $\text{SrBi}_4\text{Ti}_4\text{O}_{15}$, which parallels that found in $\text{SrBi}_2\text{Ta}_2\text{O}_9$, are discussed. © 2002 Elsevier Science (USA)

INTRODUCTION

The Aurivillius family (1) of layered bismuth-containing oxides encompasses many ferroelectric materials (2, 3), which have recently attracted considerable interest due to the observation of fatigue-free behaviour and low coercive field in thin film form (4). Hence, the representative Aurivillius-phase $\text{SrBi}_2\text{Ta}_2\text{O}_9$ is currently the material of choice for potential applications in ferroelectric random access memories (FeRAMs). Structurally, the Aurivillius phases may be considered as layered intergrowths of fluorite-like $[M_2O_2]$ units alternating with perovskite-like $[A_{n-1}B_nO_{3n+1}]$ units to give a general composition $M_2A_{n-1}B_nO_{3n+3}$, where M is generally Bi^{3+} ,

¹To whom correspondence should be addressed. E-mail: pl@st-and.ac.uk.

A is a group II or lanthanide metal, and B is a d^0 transition element (Ti^{4+} , Nb^{5+} , Ta^{5+} , etc.). For differing numbers of perovskite layers, n , typical Aurivillius phases are Bi_2WO_6 ($n=1$), $\text{SrBi}_2\text{Ta}_2\text{O}_9$ ($n=2$), $\text{Bi}_4\text{Ti}_3\text{O}_{12}$ ($n=3$), and $\text{SrBi}_4\text{Ti}_4\text{O}_{15}$ ($n=4$). We have recently carried out detailed crystallographic studies, using powder neutron diffraction (PND), on several Aurivillius phases to study two key aspects of their behavior, firstly, cation ordering at the $[M_2O_2]$ and perovskite A sites (5, 6) and, secondly, the nature of the ferroelectric–paraelectric phase transition. In the latter work, our first study consisted of a structure determination of the three-layer phase $\text{Bi}_4\text{Ti}_3\text{O}_{12}$ at the temperatures of 25, 500, 650, and 800°C, both above and below the reported ferroelectric Curie point, $T_c = 675^\circ\text{C}$. We established that the main driving force behind the ferroelectric transition was the optimization of the bonding around the Bi atom in the perovskite A site (7). On the basis of the limited number of temperatures studied in that work, we suggested a single phase transition from the ferroelectric, polar phase (space group $B2cb$) to the high-temperature, paraelectric phase (space group $I4/mmm$). In our following paper, we carried out a more detailed temperature-dependent study (at nine temperatures) of the two-layer phase $\text{Sr}_{0.85}\text{Bi}_{2.1}\text{Ta}_2\text{O}_9$. In that work (8) we established conclusively that a second phase transition occurs above the ferroelectric–paraelectric (FE–PE) transition and that the FE–PE transition itself corresponded not to an orthorhombic–tetragonal one but to an orthorhombic–orthorhombic one. Specifically, our study showed the following sequence of phases: $A2_1am$ 375°C → $Amam$ 550°C → $I4/mmm$, with a T_c of 375°C. In light of this unexpected and exciting result, we felt that a more detailed study of the temperature-dependent structural behavior of related Aurivillius phases was merited. In particular, a similar orthorhombic–orthorhombic–tetragonal phase transition sequence has been postulated, based on electron diffraction data, for the four-layer material $\text{SrBi}_4\text{Ti}_4\text{O}_{15}$ (9).

In this paper we present a detailed variable-temperature PND study of $\text{SrBi}_4\text{Ti}_4\text{O}_{15}$ and a re-analysis by PND of the related four-layer phase $\text{Bi}_5\text{Ti}_3\text{FeO}_{15}$, the structure of which has previously been reported, in a different space group, from single-crystal X-ray data (10).

EXPERIMENTAL

Approximately 10-g powder samples of $\text{SrBi}_4\text{Ti}_4\text{O}_{15}$ and $\text{Bi}_5\text{Ti}_3\text{FeO}_{15}$, suitable for PND, were prepared by solid state reaction of stoichiometric quantities of SrCO_3 , Bi_2O_3 , TiO_2 , and Fe_2O_3 . For $\text{SrBi}_4\text{Ti}_4\text{O}_{15}$ the heating sequence was $850^\circ\text{C}/24\text{ h}$, $1000^\circ\text{C}/24\text{ h}$, $1000^\circ\text{C}/24\text{ h}$; for $\text{Bi}_5\text{Ti}_3\text{FeO}_{15}$ the heating sequence was $1000^\circ\text{C}/48\text{ h}$. Preliminary powder X-ray diffraction, on a Stoe STADI/P powder diffractometer, revealed that both samples were phase pure. Additional high-resolution X-ray powder diffraction data for $\text{SrBi}_4\text{Ti}_4\text{O}_{15}$ were collected on the beamline 9.1 at the CLRC Daresbury Laboratory, U.K. The sample was enclosed in a thin-walled glass capillary (0.5-mm diameter) and data were collected over the range $3^\circ < 2\theta < 70^\circ$ at a wavelength of 1.000 \AA . Powder neutron diffraction data were collected on the high-resolution powder diffractometer HRPD (for $\text{SrBi}_4\text{Ti}_4\text{O}_{15}$) and the high-flux powder diffractometer Polaris (for $\text{Bi}_5\text{Ti}_3\text{FeO}_{15}$) at the CLRC ISIS Facility, U.K. Data were collected in a thin-walled cylindrical vanadium can at temperatures of 25, 200, 300, 400, 500, 550, 600, 650, 700, and 800°C for $\text{SrBi}_4\text{Ti}_4\text{O}_{15}$ and 25°C only for $\text{Bi}_5\text{Ti}_3\text{FeO}_{15}$, each data collection lasting approximately 2 h. The HRPD and Polaris instruments operate in time-of-flight mode, with fixed detector banks. For the Polaris data, two detector banks (90° and 145°) were employed for Rietveld refinement, giving a total data range $0.43 < d < 4.2\text{ \AA}$. For HRPD, only the data from the high-resolution “backscattering” banks ($2\theta \sim 168^\circ$) were used for Rietveld analysis, leading to a data range of $0.66 < d < 2.5\text{ \AA}$. This analysis was carried out using the GSAS suite (11).

Mössbauer spectra were collected at 25°C from a powdered sample of $\text{Bi}_5\text{Ti}_3\text{FeO}_{15}$ mounted in a conventional constant acceleration spectrometer with a 50-mCi ^{57}Co -Rh source. The isomer shift (δ) and quadrupole splitting (Δ_{EQ}) were determined for the spectrum using the software package “Recoil” (12). All the Mössbauer parameters are quoted relative to the metallic iron spectrum at room temperature.

RESULTS AND DISCUSSION

(i) Crystal Structure of $\text{Bi}_5\text{Ti}_3\text{FeO}_{15}$ at 25°C

The structure of $\text{Bi}_5\text{Ti}_3\text{FeO}_{15}$ was originally reported by Kubel and Schmid from single-crystal X-ray diffraction data on weakly twinned crystals (10). They refined the

structure in space group $Fmm2$, with $a \sim 5.43$, $b \sim 41.1$, and $c \sim 5.47\text{ \AA}$ (corresponding to $F2mm$ in the more conventional representation for layered perovskites, with c as the “unique” axis). Although polar along the a axis, in the same sense as in $A2_1am$, the higher symmetry space group allows only *displacements* along the a axis, and no tilting of the BO_6 octahedral units. Lowering of the symmetry to $A2_1am$ allows this tilting (Fig. 1) and has, in fact, been predicted as the maximum ideal symmetry for a ferroelectric Aurivillius phase with an even number of perovskite layers (13). Our analysis was therefore carried out in this lower symmetry space group, with starting coordinates being derived from those of the $Fmm2$ model, by using an origin shift of $(\frac{1}{4}, \frac{1}{4}, 0)$ to maintain a conventional setting of the space group. The best refinement included individual isotropic thermal parameters for all Bi and O atoms, resulting in 42 structural parameters and a total of 59 refined parameters. Final refined atomic parameters and selected bond distances and angles for this model are given in Tables 1 and 2, respectively. Our study confirms the previous predictions that $A2_1am$ is, in fact, the correct space group and demonstrates that the analysis of Kubel and Schmid is incorrect in this detail. This is a clear

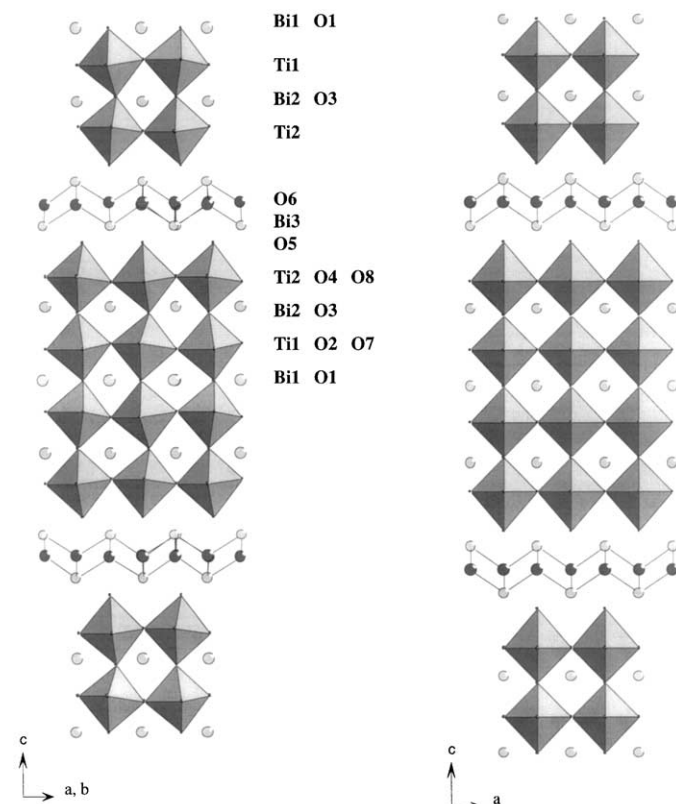
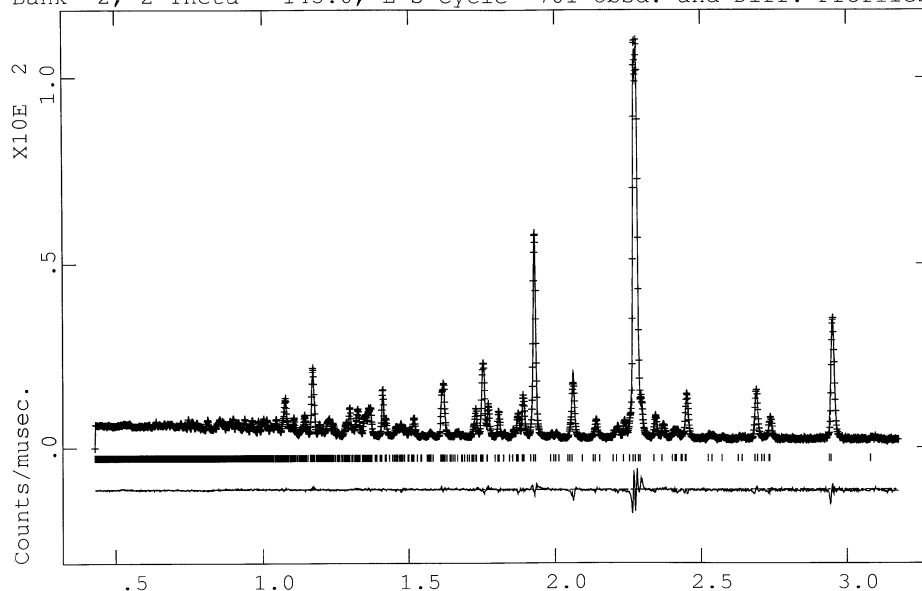


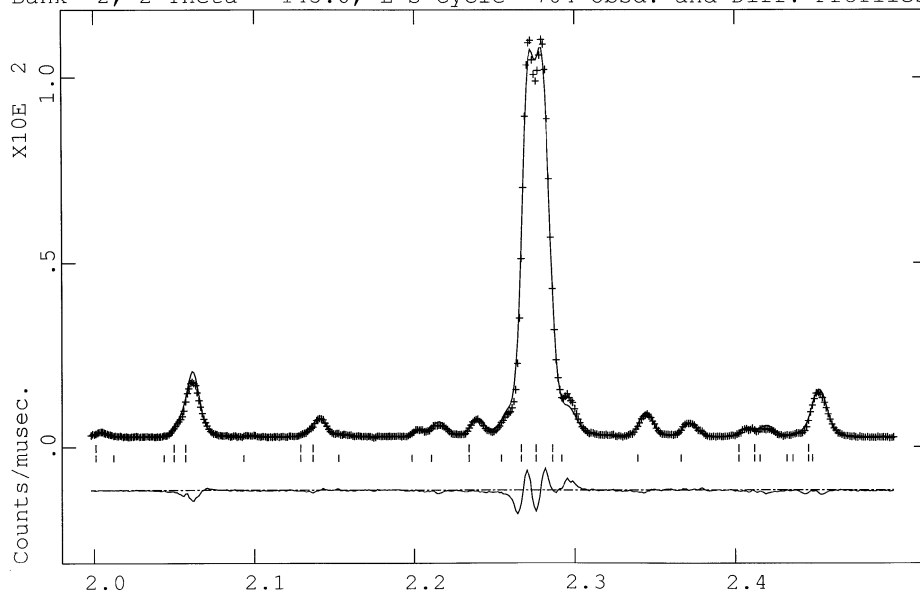
FIG. 1. Crystal structure of the archetypal four-layer Aurivillius phase: (a) space group $A2_1am$, along the $[110]$ direction, and (b) space group $I4/mmm$, along $[100]$.

Bi₅Ti₃FeO₁₅ 25C A21am Hist 2
 Bank 2, 2-Theta 145.0, L-S cycle 701 Obsd. and Diff. Profiles



(a) D-spacing, A

Bi₅Ti₃FeO₁₅ 25C A21am Hist 2
 Bank 2, 2-Theta 145.0, L-S cycle 704 Obsd. and Diff. Profiles



(b) D-spacing, A

FIG. 2. Final Rietveld plot (145° detector bank) for the refinement of Bi₅Ti₃FeO₁₅ in space group *A*₂₁*am*: (a) full data range; (b) highlight of some reflections violating *F*-centering. The bottom set of tick marks represents *A*₂₁*am*, and the top set *F*₂*mm*.

example of the advantages of neutron over X-ray diffraction methods for the precise structural analysis of heavy metal oxides of this type; i.e., the majority of the additional scattering observed in lowering the symmetry from *F*₂*mm* to *A*₂₁*am* arises from displacements of the oxygen atoms, due to the octahedral tilting mode. The effect of this octahedral tilting can be clearly seen in the final Rietveld

plot (Fig. 2) where some of the additional peaks due to the lowering of symmetry to *A*₂₁*am* are marked. We would like to point out that we located a false minimum during this refinement, which gives quite a plausible fit ($\chi^2 \sim 13$) and involves “anti-rotations” of the octahedral units; i.e., the (*x*,*y*) parameters O(2), O(4), O(7), and O(8) become “trapped” at sites oppositely displaced around the pseu-

TABLE 1

Refined Structural Parameters for Bi₅Ti₃FeO₁₅ at 25°C, Space Group *A2₁am*, *a* = 5.4698(1) Å, *b* = 5.4389(1) Å, *c* = 41.197(1) Å, *R*_{wp} = 0.032, $\chi^2 = 5.3$, for 7878 Data Points and 4632 Contributing Reflections, $0.43 < d < 4.2$ Å

Atom	<i>x</i>	<i>y</i>	<i>z</i>	<i>U</i> _{iso} (× 100)
Bi(1)	0.25 ^a	0.2494(7)	0	1.28(5)
Bi(2)	0.2381(11)	0.2446(5)	0.10453(3)	0.73(3)
Bi(3)	0.2298(8)	0.2678(5)	0.21946(4)	1.07(4)
Ti(1) ^b	0.315	0.189	0.4544	0.5
Ti(2) ^c	0.258	0.277	0.3540	0.5
O(1)	0.3362(11)	0.1771(9)	0.5	0.33(8)
O(2)	0.6074(9)	0.5460(7)	0.05182(8)	1.23(7)
O(3)	0.3250(10)	0.3060(7)	0.40504(8)	0.72(6)
O(4)	0.5326(9)	0.4854(6)	0.13844(8)	0.57(5)
O(5)	0.2911(11)	0.2034(7)	0.30494(7)	1.36(8)
O(6)	0.5045(8)	0.4888(6)	0.25061(7)	0.44(4)
O(7)	0.0334(11)	-0.0299(7)	0.03943(8)	1.16(6)
O(8)	0.0832(9)	0.0323(6)	0.14694(7)	0.43(5)

^aFixed to define origin of polar axis.

^bCoordinates and *U*_{iso} fixed from X-ray refinement. Site occupancy 0.75(1) Ti; 0.25(1) Fe.

^cCoordinates and *U*_{iso} fixed from X-ray refinement. Site occupancy 0.75(1) Ti; 0.25(1) Fe.

do-special positions (0,0) or ($\frac{1}{2}, \frac{1}{2}$). Care must therefore be taken in similar refinements so that the true minimum is found. A similar phenomenon has been highlighted in the previous single-crystal X-ray work on the *n* = 3 phase Bi₄Ti₃O₁₂ (14).

TABLE 2

Selected Bond Distances (Å) and Angles (°) for Bi₅Ti₃FeO₁₅

Bi(1)–O(1)	3.148(6)	Bi(2)–O(2)	2.554(4)
	2.374(7)		3.388(4)
	2.298(6)	Bi(2)–O(3)	2.310(5)
	3.231(6)		3.246(5)
Bi(1)–O(2) × 2	2.531(4)		2.464(5)
	3.314(4)		3.115(5)
Bi(1)–O(7) × 2	2.520(5)	Bi(2)–O(4)	2.502(5)
	2.543(5)		2.318(5)
			3.267(4)
Bi(3)–O(5)	2.606(5)	Bi(2)–O(7)	2.259(4)
	3.235(5)	Bi(2)–O(8)	2.981(4)
		3.248(4)	
	2.595(4)	O(3)–O(1)–O(3) ^a	159.6
Bi(3)–O(6)	2.313(4)	O(1)–O(3)–O(5) ^a	162.3
	2.217(4)	O(7)–O(2)–O(7) ^a	157.4
	2.233(4)	O(8)–O(4)–O(8) ^a	164.8
	2.466(4)		

Note. Distances and angles within the octahedral units are not included due to the near zero neutron scattering of the Ti/Fe position.

^aThese are the nonbonded contact angles “through” adjacent vertex-linked octahedra. Hence, O(3)–O(1)–O(3) and O(1)–O(3)–O(5) represent a measure of the tilting around the *a/b* axes; O(7)–O(2)–O(7) and O(8)–O(4)–O(8) represent tilting around the *c* axis. Note that O(2)–O(7)–O(2) and O(4)–O(8)–O(4) are symmetrically equivalent to O(7)–O(2)–O(7) and O(8)–O(4)–O(8), respectively.

Our model provides a significantly different and more accurate and precise structure than the previous analysis. For example, the typical standard error on a Bi–O bond length has been reduced from ~0.03 to ~0.005 Å in this study. More importantly, the true nature of the structure, involving tilting of octahedral *BO*₆ units, is revealed. This has a significant impact on the local environment of the three Bi sites. The octahedral tilt mode is discussed in more detail later.

The main additional question to be answered from this study, again more precisely determined from neutron rather than X-ray diffraction, is the nature of ordering of the Fe/Ti over the *B* sites of the perovskite blocks. Neutron diffraction is very sensitive to this ordering (neutron scattering lengths: *b*(Fe) = 9.5 fm, *b*(Ti) = -3.4 fm). Hence, it readily became apparent from our refinements that the Fe/Ti distribution over the two distinct *B* sites was perfectly random, within experimental error. This results in the net scattering at both these sites being almost zero, so it is impossible to define the true atomic position at these sites with any certainty. The coordinates of these sites were therefore fixed at points determined from an independent powder XRD Rietveld analysis, and the resultant bond lengths should not be taken as definitive. As a test of the validity of this model, we carried out a refinement of a “perfectly ordered” model, i.e., 100% Ti in the “outer” octahedral site and Ti(1) and 50% Ti in the “inner” site Ti(2). This refinement resulted in much poorer agreement factors ($\chi \sim 35$, compared with 5.3 for the disordered model). In an effort to improve the precision of the *B* cation positions, we also carried out *simultaneous* refinements against both neutron and X-ray powder data; these refinements did not significantly enhance the model. Thus, although we can state conclusively that the Fe/Ti distribution is random, we cannot infer the precise *local* coordination around either Fe or Ti from these data. This is rather an interesting subtlety since it may be expected that Ti would prefer to lie “off-center” in its site due to the second-order Jahn–Teller effect (15) and may therefore prefer the “outer” site, which is inherently more distorted in previous structure determinations of Aurivillius phases. An ordering of *d*⁰ versus *d*^{II} cations in the Aurivillius-phase Bi₂Sr₂Nb₂MnO_{12-x} (16) and in the related Ruddlesden–Popper-phase Na₂La₂Ti₂RuO₁₀ (17) has indeed been reported and in the latter case was ascribed to this effect. To probe the local environment of the iron atoms further, we collected ⁵⁷Fe Mossbauer data on Bi₅Ti₃FeO₁₅.

The Mössbauer spectrum collected at 25°C is shown as solid circles in Fig. 3. The best fit to the data is by two quadrupole split doublets with $\delta = 0.248(5)$ and $0.239(5)$ mms⁻¹ and $\Delta_{EQ} = 0.47(2)$ and $0.67(3)$ mms⁻¹. The need for two sub components shows the presence of two Fe sites in the structure and the relative areas of the two doublets (51% and 49%) indicate that the sites are approximately

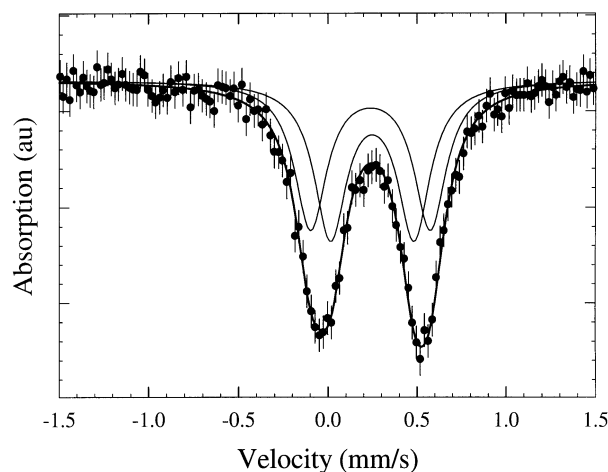


FIG. 3. Mössbauer spectra collected from $\text{Bi}_5\text{Ti}_3\text{FeO}_{15}$ at 25°C . The data are shown as filled circles and the fit and subspectra as solid lines.

equally occupied, in agreement with the Rietveld refinement. In Mössbauer spectroscopy the size of the isomer shift is a result of both the coordination and valence of the iron in the material under investigation, and the quadrupole splitting arises from the interaction between the nuclear quadrupole moment and a non-zero electric field gradient at the nucleus. The size of the quadrupole splitting is determined by valence electrons and ligands and therefore provides information on the oxidation state, coordination number, and site distortion. Values of $\delta \sim 0.25 \text{ mms}^{-1}$ and Δ_{EQ} of $\sim 0.6 \text{ mms}^{-1}$ are typical of Fe^{3+} ions in an octahedral environment (18). Therefore, we can say that in $\text{Bi}_5\text{Ti}_3\text{FeO}_{15}$ there are two iron sites, both Fe^{3+} , surrounded by a distorted octahedron of oxygen atoms, but having differing degrees of distortion. The final fit based on this model is shown in Fig. 3.

(ii) Crystal Structure of $\text{SrBi}_4\text{Ti}_4\text{O}_{15}$ at 25°C

The precise crystal structure of this phase has never been reported previously. Since preliminary inspection of the raw PND data at 25°C clearly showed an A -centered, rather than an F -centered cell (see later), our analysis began using the model described above, in space group $A2_1am$, which is in line with Newnham's hypothesis for phases of this type (13). Due to the relative similarities in neutron scattering lengths for Sr and Bi (7.02 and 8.53 fm, respectively), it was first necessary to establish the ordering of these two cations over the three available sites using powder X-ray data. Refinements of this approximate model (positions of oxygen atoms were not refined) against the synchrotron data clearly showed that there was no significant occupancy of the $[M_2O_2]$ layers by Sr and that the two distinct A sites were randomly occupied by Sr. In all the subsequent refinements of the PND data, the

TABLE 3

Refined Structural Parameters for $\text{SrBi}_4\text{Ti}_4\text{O}_{15}$ at 25°C , Space Group $A2_1am$, $a=5.4507(1) \text{ \AA}$, $b=5.4376(1) \text{ \AA}$, $c=40.9841(8) \text{ \AA}$, $R_{\text{wp}}=0.104$, $\chi=6.1$, for 4403 Data Points and 1738 Contributing Reflections, $0.66 < d < 2.5 \text{ \AA}$

Atom	x	y	z	$U_{\text{iso}} (\times 100)$
Bi(1) ^b	0.25 ^a	0.258(2)	0	3.3(2)
Bi(2) ^b	0.255(3)	0.248(1)	0.10409(10)	4.3(1)
Bi(3)	0.245(2)	0.263(1)	0.21881(9)	3.5(1)
Ti(1)	0.277(3)	0.250(3)	0.45032(14)	1.0(1)
Ti(2)	0.268(3)	0.242(2)	0.34697(16)	1.7(2)
O(1)	0.306(3)	0.203(3)	0.5	4.5(4)
O(2)	0.580(3)	0.538(3)	0.0515(2)	2.8(2)
O(3)	0.301(3)	0.298(2)	0.40348(14)	2.6(2)
O(4)	0.523(2)	0.495(2)	0.14058(14)	1.2(2)
O(5)	0.286(3)	0.212(2)	0.30456(14)	3.2(2)
O(6)	0.510(3)	0.498(2)	0.2502(2)	2.3(2)
O(7)	0.017(4)	-0.019(2)	0.0433(2)	4.7(3)
O(8)	0.047(2)	0.016(2)	0.1479(2)	4.1(2)

^aFixed to define origin of polar axis.

^bComposition fixed at 0.67Bi/0.33Sr.

occupancies of the A sites were therefore fixed at 0.33Sr/0.67Bi. The final model at 25°C in space group $A2_1am$ involved isotropic refinement of all atoms, resulting in 49 variable structural parameters and 60 total refined parameters. Final refined atomic coordinates/thermal parameters and selected bond distances are given in Tables 3 and 4, respectively.

TABLE 4

Selected Bond Distances (\AA) for $\text{SrBi}_4\text{Ti}_4\text{O}_{15}$ at 25°C

Bi(1)–O(1)	3.03(2)	Bi(2)–O(2)	2.63(1)
	2.44(2)		3.20(1)
	2.43(2)	Bi(2)–O(3)	2.51(1)
	3.04(2)		3.00(1)
Bi(1)–O(2) $\times 2$	3.16(1)		2.48(1)
$\times 2$	2.56(1)		3.02(1)
Bi(1)–O(7) $\times 2$	2.65(2)	Bi(2)–O(4)	2.48(1)
$\times 2$	2.64(2)		2.41(1)
		Bi(2)–O(7)	3.16(1)
			3.13(1)
Bi(3)–O(5)	2.68(1)	Bi(2)–O(8)	2.47(1)
	3.11(1)		2.79(1)
	3.16(1)		
	2.63(1)	Ti(1)–O(1)	2.058(6)
Bi(3)–O(6)	2.32(1)	Ti(1)–O(2)	1.90(2)
	2.23(1)		2.01(2)
	2.29(1)	Ti(1)–O(3)	1.941(8)
	2.41(1)	Ti(1)–O(7)	1.98(2)
			1.91(2)
Ti(2)–O(3)	2.343(8)		
Ti(2)–O(4)	1.93(2)		
	2.00(2)		
Ti(2)–O(5)	1.749(8)		
Ti(2)–O(8)	2.02(2)		
	1.93(2)		

SrBi₄Ti₄O₁₅ adopts the same space group, and therefore the same type of octahedral tilt system as Bi₅Ti₃FeO₁₅, though in the latter case the orthorhombic distortion is slightly larger due to the slightly lower tolerance factor within the perovskite block. In our previous work on both two-layer system $ABi_2Nb_2O_9$ ($A = \text{Ca, Sr, Ba}$) (5) and the three-layer system $Bi_{2-x}Sr_{2+x}Ti_{1-x}Nb_{2+x}O_{12}$ ($0 < x < 0.8$) (6), we have shown that a certain degree of cation disorder exists between the perovskite A site and the $[M_2O_2]$ layer. We have rationalized this on the basis of a compensation of the size mismatch of the $[M_2O_2]$ and the $[A_{n-1}B_nO_{3n+1}]$ layer, such that, as the size of the A cation increases, the perovskite block becomes “too wide” to intergrow compatibly with the fluorite block, and cation disorder ensues, which increases with the size mismatch, i.e. the increasing size of A . The observation of no significant cation disorder of this type in the present system is in agreement with our earlier hypothesis since the $[\text{SrBi}_2\text{Ti}_4\text{O}_{13}]$ unit is relatively “narrow” compared to those we studied previously; hence, the size mismatch is correspondingly small. This can be seen by a comparison of the a/b lattice parameters in the present case ($a = 5.451 \text{ \AA}$ and $b = 5.438 \text{ \AA}$) with those in $\text{Bi}_2\text{Sr}_2\text{TiNb}_2\text{O}_{12}$ (6) ($a = b = 5.503 \text{ \AA}$) and $\text{CaBi}_2\text{Nb}_2\text{O}_9$ (5) ($a = 5.483 \text{ \AA}$ and $b = 5.442 \text{ \AA}$), where cation disorder of the order 20% and 5%, respectively occurs. As might be expected due to the accommodation of Sr^{2+} in the A sites, the a/b lattice parameters in the present case are larger and the degree of orthorhombic distortion is smaller than what occurs in the the three-layer phase $\text{Bi}_4\text{Ti}_3\text{O}_{12}$ (7) ($a = 5.444 \text{ \AA}$ and $b = 5.409 \text{ \AA}$).

Systems of octahedral tilts in three-dimensional perovskites have been classified in the well-known papers of Glazer (19) and, more recently, by Woodward (20). A similar analysis, though with a differing notation, for layered perovskites has been given by Aleksandrov and Bartolomi (21). Aleksandrov and Bartolomi’s system correctly predicts the space group $A2_1am$ for the two-layer Aurivillius phases, e.g., $\text{SrBi}_2\text{Ta}_2\text{O}_9$, which he classifies as a $(\Phi\Phi\Psi_z)$ system. Aleksandrov and Bartolome’s suggests that all “even-layered” Aurivillius phases should adopt this same system. In this notation Φ corresponds to adjacent octahedra having the same magnitude of tilt but the *opposite* direction of tilt along a given crystallographic axis, whereas Ψ corresponds to the *same* direction of tilt for adjacent octahedra. This situation is analogous to the three-dimensional tilt system $a^+b^-b^-$ in the Glazer notation. The assignment of the $(\Phi\Phi\Psi_z)$ tilt to the two-layer systems is unambiguous since the mirror plane perpendicular to c between the two octahedra necessitates a Ψ -type rather than a Φ -type tilt. However, in the four-layer systems the same $A2_1am$ space group does *not necessarily* imply a $(\Phi\Phi\Psi_z)$ tilt system. There seems to be an inherent ambiguity in this notation since the mirror

plane perpendicular to c does not constrain the $\text{Ti}(1)\text{O}_6$ and $\text{Ti}(2)\text{O}_6$ octahedra to rotate in phase with each other. In fact, as shown in Fig. 4, these octahedra are in *anti-phase* to each other in our system, while the $\text{Ti}(1)\text{O}_6/\text{Ti}(1)\text{O}_6$ and $\text{Ti}(2)\text{O}_6/\text{Ti}(2)\text{O}_6$ pairs are constrained to be *in-phase*. Hence the tilt system within the four-layer block, relative to the c -axis could more precisely be described as $\text{Ti}(2)-(\Phi)-\text{Ti}(1)-(\Psi)-\text{Ti}(1)-(\Phi)-\text{Ti}(2)$ in the Aleksandrov-like notation or $\text{Ti}(2)-(-)-\text{Ti}(1)-(+)-\text{Ti}(1)-(-)-\text{Ti}(2)$ in the Glazer-like notation.

Finally, a simple calculation of the total spontaneous polarization for $\text{SrBi}_4\text{Ti}_4\text{O}_{15}$ at room temperature, using the point charge model (see, for example, Shimakawa *et al.* (22)) gives $P_s = 23.2 \mu\text{C cm}^{-2}$. In Table 3 it can be seen that (i) the $\text{Bi}(2)$, $\text{Bi}(3)$, and $\text{O}(6)$ atoms are displaced only very slightly along the a -axis from their ideal positions, relative to the fixed origin of $\text{Bi}(1)$, and (ii) all the Ti and remaining O atoms are displaced to a significantly greater extent by a positive Δx value; the net polarization can therefore be described as arising from a large a -axis displacement of the A -site atoms relative to their octahedral environment, with the opposite displacement of the B sites to some extent cancelling this large charge separation. The displacement of the A sites relative to the octahedra can also be seen clearly in Fig. 4. This mechanism for the behavior of the

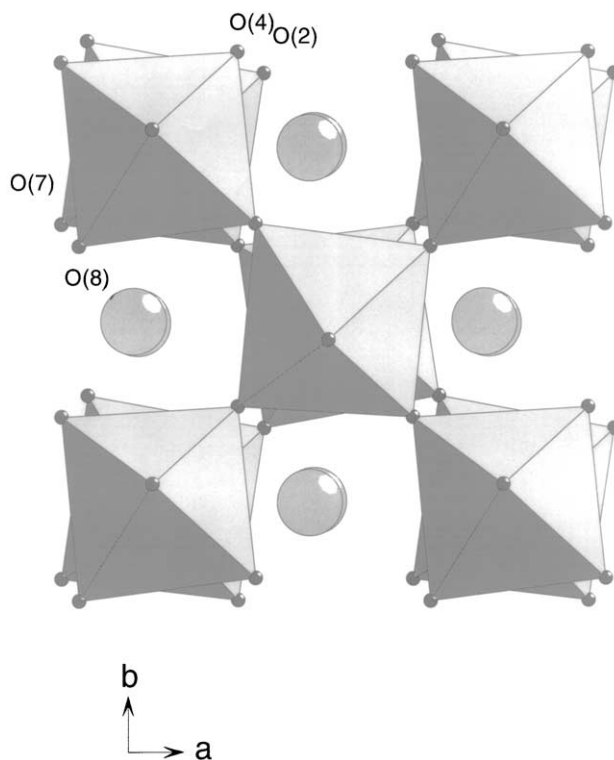


FIG. 4. Projection of a portion of the perovskite block in the $A2_1am$ phase along $[001]$, showing antiphase rotations of adjacent $\text{Ti}(2)\text{O}_6$ and $\text{Ti}(1)\text{O}_6$ octahedra, and displacements of the A -sites cations along $[100]$.

ferroelectric state is directly analogous to that suggested by Withers *et al.* (14, 23) in their work on the $n=2$ and $n=3$ Aurivillius-phases $\text{Bi}_3\text{TiNbO}_9$ and $\text{Bi}_4\text{Ti}_3\text{O}_{12}$.

(iii) *Variable Temperature Study of $\text{SrBi}_4\text{Ti}_4\text{O}_{15}$*

Refinements of each of the variable-temperature data sets were carried out in two models, *viz.* the $A2_1am$ model, with all atoms refined isotropically (resulting in 49 variable structural parameters, and 60 total refined parameters) and the “parent” $I4/mmm$ model, with all atoms refined anisotropically (resulting in 32 structural parameters and 44 total refined parameters). The resulting goodness-of-fit indices (χ^2) are given in Table 5. Three additional factors were used in determining which space group was the best choice at each temperature: (i) The previously reported Curie temperature for stoichiometric $\text{SrBi}_4\text{Ti}_4\text{O}_{15}$ is in the region 520–570°C; (ii) lattice parameters as a function of temperature show a convergence of a/b near 550°C (Fig. 5); (iii) the disappearance of several characteristic “ A -centered” reflections versus temperature can be seen from the final Rietveld plots (Fig. 6). These results together demonstrate convincingly that the $I4/mmm$ model is valid at 650°C and above, whereas $A2_1am$ is the best description of the structure below 550°C.

Interestingly, the crystallographic transition from polar orthorhombic ($A2_1am$) to centric tetragonal ($I4/mmm$), as manifested in the merging of the a/b lattice parameters and the inflection in the c axis, appears to coincide closely with the reported ferroelectric Curie point ($T_c \sim 570^\circ\text{C}$ (9) or 520°C (24)). However, a very careful look at the Rietveld difference plots for the $I4/mmm$ refinements at 550 and 600°C (Fig. 6) reveal that very weak reflections that violate the A -centering still exist at these temperatures, but

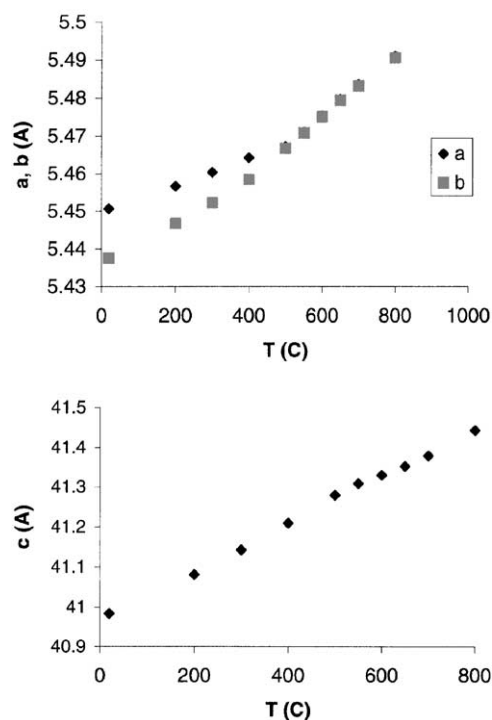


FIG. 5. Thermal evolution of lattice parameters for $\text{SrBi}_4\text{Ti}_4\text{O}_{15}$. Note that the merging of the a/b parameters coincides with a change of slope of c vs T at $\sim 550^\circ\text{C}$.

effectively disappear at 650°C. This clearly suggests that an intermediate paraelectric-but-orthorhombic phase (probable space group $Amam$) exists in this temperature interval, analogous to what we recently reported in the two-layer phase $\text{Sr}_{0.85}\text{Bi}_{2.1}\text{Ta}_2\text{O}_9$ (8). Indeed, a suggestion of a possible intermediate orthorhombic phase in SrBi_4

TABLE 6

Refined Structural Parameters for $\text{SrBi}_4\text{Ti}_4\text{O}_{15}$ at 650°C , Space Group $I4/mmm$, $a = 3.87469(4)$ Å, $c = 41.3523(5)$ Å. $R_{wp} = 0.052$, $\chi^2 = 2.4$, for 4403 Data Points and 573 Contributing Reflections, $0.66 > d > 2.5$ Å

Temp (°C)	χ^2 ($A2_1am$, iso) ^a	χ^2 ($I4/mmm$, iso) ^b	χ^2 ($I4/mmm$, anis) ^c	χ^2 ($Amam$, anis) ^d
25	6.1	19.0	16.3	
200	3.6	6.4	4.6	
300	3.5	5.5	3.6	
400	2.2	2.7	1.8	
500	3.5	4.1	2.4	
550	3.6	4.0	2.3	3.5
600	3.7	4.0	2.3	
650	3.9	4.1	2.4	
700	4.0	4.2	2.6	
800	3.9	4.1	2.4	

Atom	x	y	z	$U_{11} (\times 100)$	$U_{22} (\times 100)$	$U_{33} (\times 100)$
Bi(1) ^a	0	0	0	5.6(4)	5.6(4)	6.6(6)
Bi(2) ^a	0	0	0.2184(2)	7.5(3)	7.5(3)	7.2(4)
Ti(1)	0	0	0.4509(3)	2.7(4)	2.7(4)	4.4(5)
Ti(2)	0	0	0.3481(2)	1.0(3)	1.0(3)	3.5(5)
O(1)	0	0	0.5	8.4(7)	8.4(7)	2.9(7)
O(2) ^b	0	0.5	0.0491(3)	5.7(4)	11.8(6)	11.5(6)
O(3)	0	0	0.4052(2)	7.2(4)	7.2(4)	4.3(5)
O(4) ^c	0	0.5	0.1444(2)	1.5(3)	5.8(4)	3.5(3)
O(5)	0	0	0.3045(3)	6.6(4)	6.6(4)	6.7(6)
O(6)	0	0.5	0.25	2.6(3)	2.6(3)	8.7(7)

^a60 variables.

^b29 variables.

^c44 variables.

^d67 variables.

^aComposition fixed at 0.67Bi/0.33 Sr.

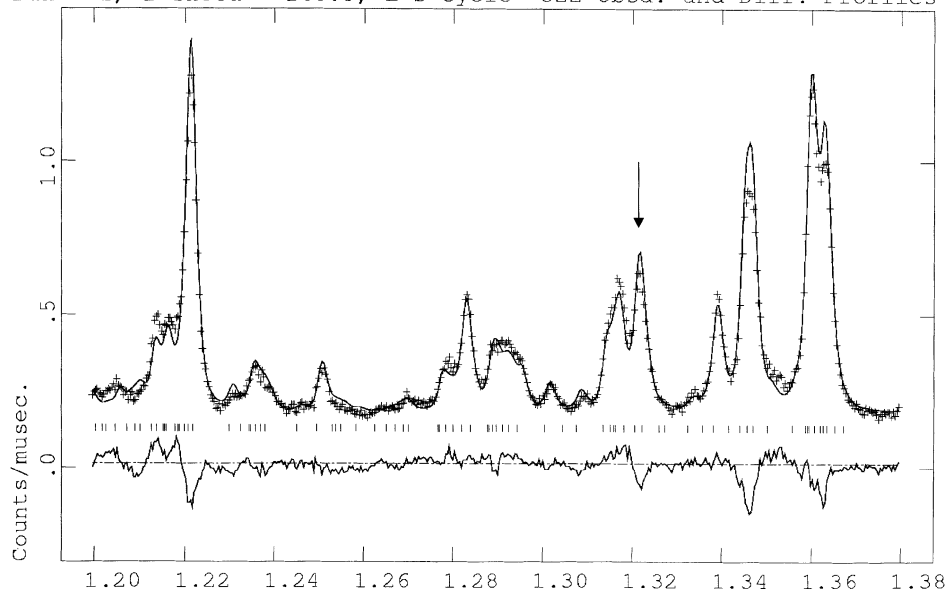
^bEquivalent to O(2) and O(7) in $A2_1am$.

^cEquivalent to O(4) and O(8) in $A2_1am$.

Ti_4O_{15} itself has been made previously from TEM studies (9). Refinements in space group $A2_1am$ were attempted for our 550 and 600°C data and led to fits which clearly accounted for the peak at $d \sim 1.33 \text{ \AA}$. However, depending on the exact nature of the refinement model (isotropic vs anisotropic, etc.), it was not possible to distinguish

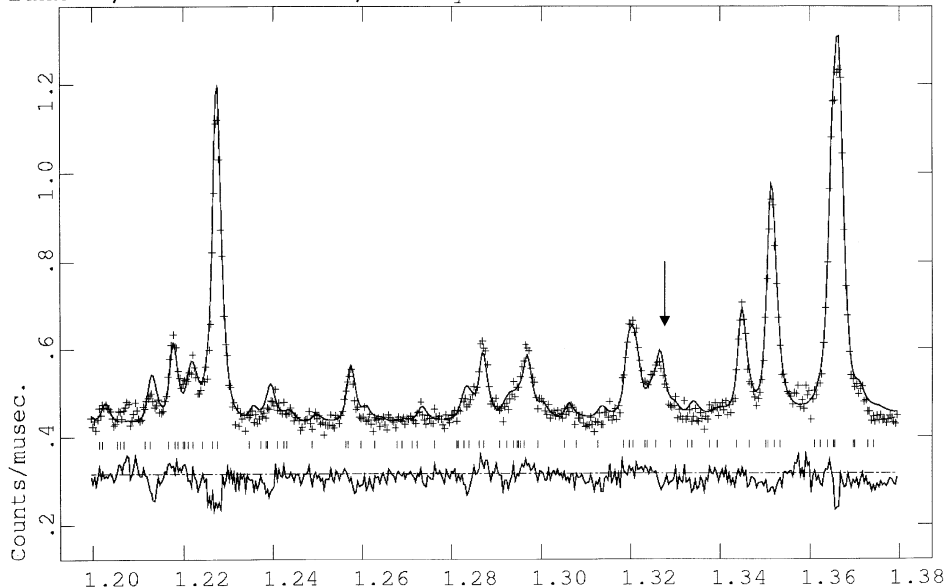
conclusively between the space groups $A2_1am$, Amm , and $I4/mmm$ based on these data alone (Table 5). Hence, although we can confirm the existence of an intermediate centrosymmetric orthorhombic phase over a small temperature interval above T_c , this is clearly a much less pronounced phenomenon than in the two-layer phase

Bi₄SrTi₄O₁₅ A2₁am RT Hist 1
Bank 1, 2-Theta 168.3, L-S cycle 522 Obsd. and Diff. Profiles



(a) D-spacing, Å

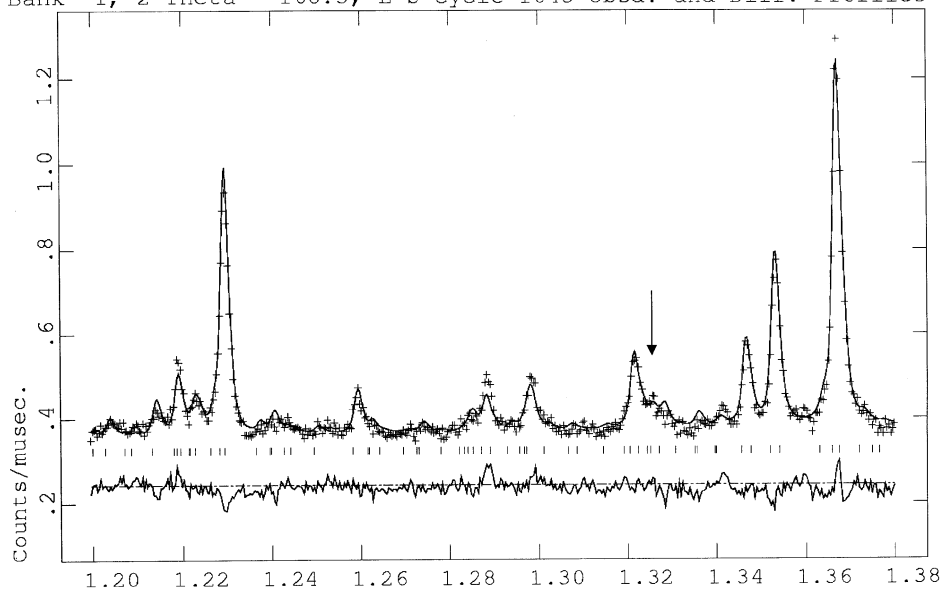
Bi₄SrTi₄O₁₅ A2₁am 400C Hist 1
Bank 1, 2-Theta 168.3, L-S cycle 874 Obsd. and Diff. Profiles



(b) D-spacing, Å

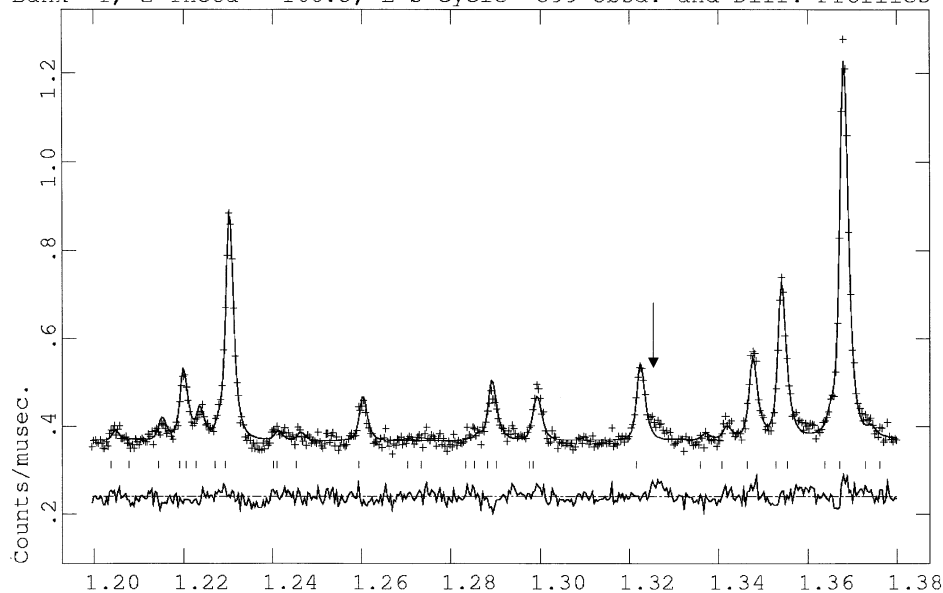
FIG. 6. Portion of the final Rietveld plot $\text{SrBi}_4\text{Ti}_4\text{O}_{15}$ versus temperature, showing the disappearance of the $411/2315/140$ reflections due to the $A2_1am$ - $I4/mmm$ transition. (a) $A2_1am$ at 25°C; (b) $A2_1am$ at 400°C; (c) $A2_1am$ at 500°C; (d) $I4/mmm$ at 550°C; (e) $I4/mmm$ at 600°C; (f) $I4/mmm$ at 650°C. The plots in (d) and (e) are shown using the $I4/mmm$ rather than the true Amm model to emphasize the continuing presence of these key reflections above T_c .

Bi₄SrTi₄O₁₅ A2₁am 500C Hist 1
 Bank 1, 2-Theta 168.3, L-S cycle 1043 Obsd. and Diff. Profiles



(c) D-spacing, Å

Bi₄SrTi₄O₁₅ I4/mmm 550C Hist 1
 Bank 1, 2-Theta 168.3, L-S cycle 599 Obsd. and Diff. Profiles



(d) D-spacing, Å

FIG. 6—Continued.

$\text{Sr}_{0.85}\text{Bi}_{2.1}\text{Ta}_2\text{O}_9$, and it was found impossible to obtain meaningful refinements of the $A_{21}am$ model, which deviated significantly from tetragonal symmetry, using the present data.

Final refined atomic coordinates for $\text{SrBi}_4\text{Ti}_4\text{O}_{15}$ at 650°C are given in Table 6 and selected bond lengths are given in Table 7. The structure of this paraelectric parent phase, in $I4/mmm$, is compared to that of the ferroelectric

phase in Fig. 1. The structure at temperatures within the $A_{21}am$ regime shows a gradual reduction of the octahedral tilting modes, as manifested in interoctahedral nonbonded O—O—O angles (Fig. 7), and a gradual increase of symmetry around each of the Bi sites, most clearly seen in the Bi(3)—O(5) lengths (Fig. 8) with increasing temperature. Interestingly, the local environment around each of the two Ti sites does not change substantially with temperature, the

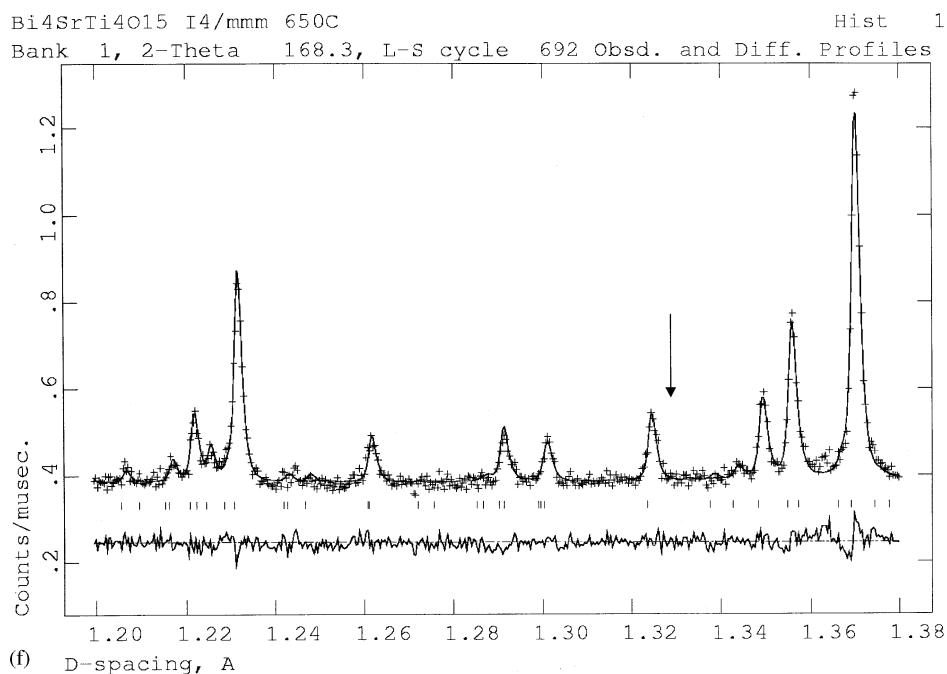
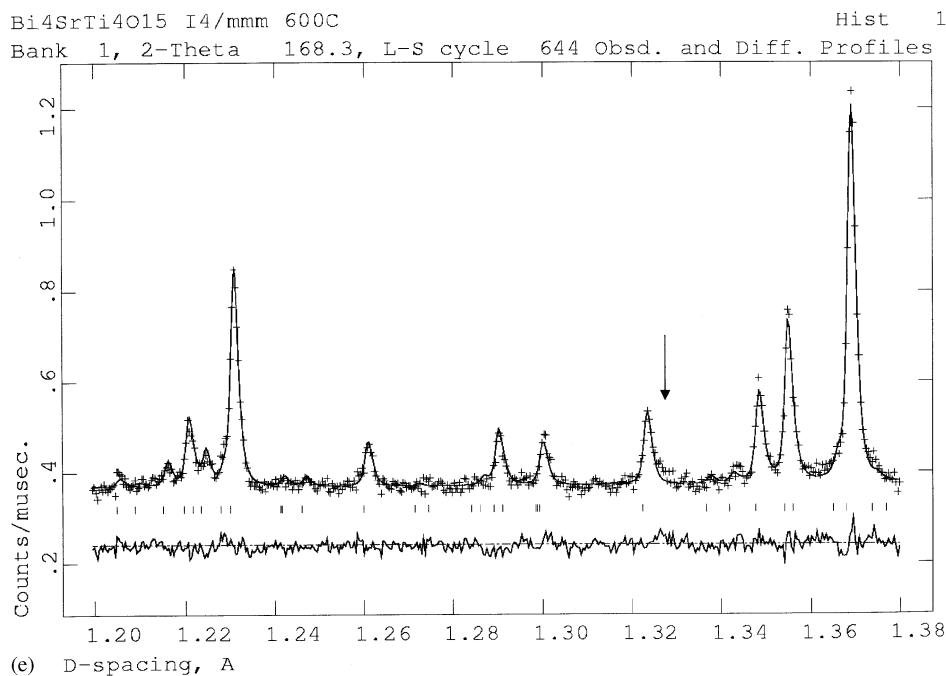


FIG. 6—Continued.

pronounced off-center displacement of Ti(2) being retained above the phase transition (Tables 4 and 7). This, of course, does not influence the ferroelectric properties directly, as there is no *net* polarization along the *c* axis arising from this local polarization. From the anisotropic refinements of the *I4/mmm* phase above 600°C (Table 6), it is apparent that there is some degree of remanent *localized* tilting of the BO_6 octahedral units, particularly the central

Ti(1) layer — as manifested, for example, in the slightly large *U* values for O(1) and O(2).

SUMMARY AND CONCLUSIONS

We have undertaken the first detailed structure refinements of four-layer Aurivillius-phase ferroelectrics using powder neutron diffraction. The refinements of both

TABLE 7
Selected Bond Distances (Å) for $\text{SrBi}_4\text{Ti}_4\text{O}_{15}$ at 650°C

$\text{Bi}(1)\text{--O}(1) \times 4$	2.73982(3)	$\text{Bi}(2)\text{--O}(2) \times 4$	2.98(1)
$\text{Bi}(1)\text{--O}(2) \times 8$	2.805(9)	$\text{Bi}(2)\text{--O}(3) \times 4$	2.765(2)
		$\text{Bi}(2)\text{--O}(4) \times 4$	2.566(9)
$\text{Bi}(3)\text{--O}(5) \times 4$	2.935(4)		
$\text{Bi}(3)\text{--O}(6) \times 4$	2.27847(2)		
$\text{Ti}(1)\text{--O}(1)$	2.03(1)	$\text{Ti}(2)\text{--O}(3)$	2.36(1)
$\text{Ti}(1)\text{--O}(2) \times 4$	1.93734(2)	$\text{Ti}(2)\text{--O}(4) \times 4$	1.962(2)
$\text{Ti}(1)\text{--O}(3)$	1.89(1)	$\text{Ti}(2)\text{--O}(5)$	1.81(1)

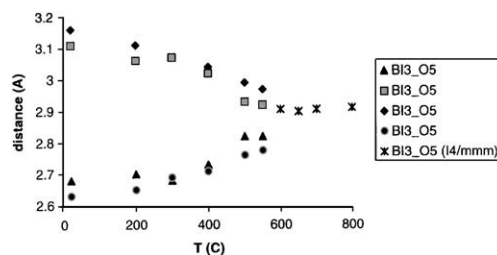


FIG. 8. Thermal evolution of the $\text{Bi}(3)\text{--O}(5)$ bond length, i.e., the link between the $[\text{Bi}_2\text{O}_2]$ layer and the apical oxygen of the perovskite block.

$\text{SrBi}_4\text{Ti}_4\text{O}_{15}$ and $\text{Bi}_5\text{Ti}_3\text{FeO}_{15}$ at 25°C convincingly demonstrate the correct space group for the ferroelectric phase to be $A2_1am$, in contrast to $F2mm$, which has been suggested by a previous single-crystal X-ray study on $\text{Bi}_5\text{Ti}_3\text{FeO}_{15}$. This lower symmetry space group permits significant tilting of the octahedral BO_6 units within the perovskite layer. This further implies that the origin of ferroelectricity in these phases is similar to that observed in two- and three-layer Aurivillius phases and lies in the bonding requirements of the perovskite A -site cations, which displace from their ideal sites in a polar manner, leading to a cooperative tilting of the octahedra. The tilting can be described in terms of *anti-phase* rotation of adjacent octahedra within the ab plane, but a combination of *in-phase* and *anti-phase* rotation of adjacent layers around the c axis; these rotations within a single quadruple perovskite unit, $\text{Ti}(2)\text{--Ti}(1)\text{--Ti}(1)\text{--Ti}(2)$, can be written as $(-)(+)(-)$ in a notation analogous to that used by Glazer. In $\text{Bi}_5\text{Ti}_3\text{FeO}_{15}$ it has been determined from both the neutron refinements and Mössbauer spectroscopy that the Fe and Ti are randomly disordered over the two available octahedral sites. In $\text{SrBi}_4\text{Ti}_4\text{O}_{15}$ it is shown that the high-temperature paraelectric phase (above 650°C) adopts the expected tetragonal symmetry, space group $I4/mmm$. However, there is firm evidence from the raw neutron diffraction data that a very subtle secondary phase transition to a paraelectric orthorhombic phase (space group Amam) occurs in the region $550 - 650^\circ\text{C}$. This transition is,

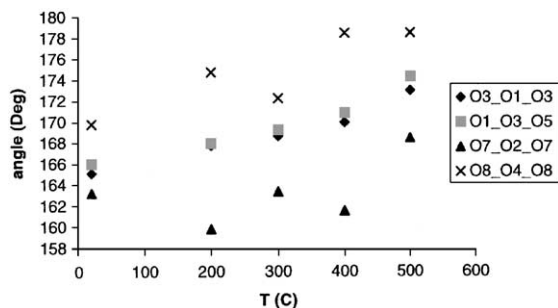


FIG. 7. Thermal evolution of the key interoctahedral O–O–O angles. See also footnote, Table 2.

however, much more subtle than that which has been shown unambiguously in the two-layer phase $\text{Sr}_{0.85}\text{Bi}_{2.1}\text{Ta}_2\text{O}_9$.

In addition to the suggestions of an intermediate paraelectric orthorhombic phase by Reaney and Damjanovic (9), we note that the birefringence studies of Kubel and Schmid (10) clearly suggested two high-temperature phase transitions in $\text{Bi}_5\text{Ti}_3\text{FeO}_{15}$, at 560 and 750°C , the first of which they ascribed to an orthorhombic–orthorhombic ($Fmm2\text{--}Fmmm$) one. Although we have now shown this space group assignment for the room-temperature phase to be incorrect, a high-temperature PND study of this material would clearly be of interest to clarify the presence and nature of the intermediate paraelectric orthorhombic phase.

ACKNOWLEDGMENTS

We thank EPSRC for Studentships (C.H.H. and A.S.) and for provision of neutron diffraction facilities at ISIS. We thank the University of St. Andrews for additional funding. We thank Dr. A. M. Kusainova, Dr. K. S. Knight, and Dr. R. M. Ibberson for help in the neutron data collection.

REFERENCES

1. B. Aurivillius, *Ark. Kemi* **1**, 499 (1949).
2. G. A. Smolenskii, V. A. Isupov, and A. I. Agranovskaya, *Sov. Phys. Solid State (Engl. Transl.)* **3**, 651 (1959).
3. E. C. Subbarao, *J. Phys. Chem. Solids* **23**, 665 (1962).
4. C. A. P. de Araujo, J. D. Cuchlaro, L. D. McMillan, M. Scott, and J. F. Scott, *Nature (London)* **374**, 627 (1995).
5. S. M. Blake, M. J. Falconer, M. McCreedy, and P. Lightfoot, *J. Mater. Chem.* **7**, 1609 (1997).
6. C. H. Hervoches and P. Lightfoot, *J. Solid State Chem.* **153**, 66 (2000).
7. C. H. Hervoches and P. Lightfoot, *Chem. Mater.* **11**, 3359 (1999).
8. C. H. Hervoches, J. T. S. Irvine, and P. Lightfoot, *Phys. Rev. B* **64**, 100102(R) (2001).
9. I. M. Reaney and D. Damjanovic, *J. Appl. Phys.* **80**, 4223 (1996).
10. F. Kubel and H. Schmid, *Ferroelectrics* **129**, 101 (1992).
11. A. C. Larson and R. B. von Dreele, Los Alamos National Laboratory Report No. LA-UR-86-748, 1987.
12. K. Lagarec and D. G. Rancourt, "Recoil, Mössbauer spectral analysis software for Windows," University of Ottawa, 1998.
13. R. E. Newham, R. W. Wolfe, and J. F. Dorrian, *Mater. Res. Bull.* **6**, 1029 (1971).
14. A. D. Rae, J. G. Thompson, R. L. Withers, and A. C. Willis, *Acta Crystallogr. B* **46**, 474 (1990).

15. N. S. P. Bhuvanesh and J. Gopalakrishnan, *J. Mater. Chem.* **7**, 2297 (1997).
16. W. J. Yu, Y. I. Kim, D. H. Ha, J. H. Lee, Y. K. Park, S. Seong, and N. H. Hur, *Solid State Commun.* **111**, 705 (1999).
17. J. N. Lalena, A. U. Falster, W. B. Simmons, E. E. Carpenter, J. Wiggins, S. Hariharan, and J. B. Wiley, *Chem. Mater.* **12**, 2418 (2000).
18. F. Menil, *J. Phys. Chem. Solids* **46**, 763 (1985).
19. A. M. Glazer, *Acta Crystallogr. B* **28**, 3384 (1972).
20. P. M. Woodward, *Acta Crystallogr. B* **53**, 32 (1997).
21. K. S. Aleksandrov and J. Bartolomé, *J. Phys. Condens. Matter* **6**, 8219 (1994).
22. Y. Shimakawa, Y. Kubo, Y. Nakagawa, T. Kamiyama, H. Asano, and F. Izumi, *Appl. Phys. Lett.* **74**, 1904 (1999).
23. R. L. Withers, J. G. Thompson, and A. D. Rae, *J. Solid State Chem.* **94**, 404 (1991).
24. Y. Noguchi, M. Miyayama, and T. Kudo, *Appl. Phys. Lett.* **77**, 3639 (2000).